



You have downloaded a document from  
**RE-BUŚ**  
repository of the University of Silesia in Katowice

**Title:** Two stages of Late Carboniferous to Triassic magmatism in the Strandja Zone of Bulgaria and Turkey

**Author:** Anna Sałacińska, Ianko Gerdjikov, Ashley Gumsley, Krzysztof Szopa, David Chew, Aleksandra Gawęda, Izabela Kocjan

**Citation style:** Sałacińska Anna, Gerdjikov Ianko, Gumsley Ashley, Szopa Krzysztof, Chew David, Gawęda Aleksandra, Kocjan Izabela. (2021). Two stages of Late Carboniferous to Triassic magmatism in the Strandja Zone of Bulgaria and Turkey. "Geological Magazine" (Vol. 0, iss. 0 (2021), s. 1-14), DOI: 10.1017/S0016756821000650



Uznanie autorstwa - Licencja ta pozwala na kopiowanie, zmienianie, rozprowadzanie, przedstawianie i wykonywanie utworu jedynie pod warunkiem oznaczenia autorstwa.



UNIwersYTET ŚLĄSKI  
W KATOWICACH



Biblioteka  
Uniwersytetu Śląskiego



Ministerstwo Nauki  
i Szkolnictwa Wyższego

## Original Article

**Cite this article:** Sałacińska A, Gerdjikov I, Gumsley A, Szopa K, Chew D, Gawęda A, and Kocjan I. Two stages of Late Carboniferous to Triassic magmatism in the Strandja Zone of Bulgaria and Turkey. *Geological Magazine* <https://doi.org/10.1017/S0016756821000650>

Received: 9 February 2021

Revised: 3 June 2021

Accepted: 8 June 2021

**Keywords:**

Strandja Zone; Sakar unit; U–Pb zircon dating; Izvorovo Pluton

**Author for correspondence:**

Anna Sałacińska,  
Email: [anna.salacinska@twarda.pan.pl](mailto:anna.salacinska@twarda.pan.pl)

# Two stages of Late Carboniferous to Triassic magmatism in the Strandja Zone of Bulgaria and Turkey

Anna Sałacińska<sup>1,2</sup> , Ianko Gerdjikov<sup>3</sup>, Ashley Gumsley<sup>1</sup>, Krzysztof Szopa<sup>1</sup>, David Chew<sup>4</sup>, Aleksandra Gawęda<sup>1</sup> and Izabela Kocjan<sup>2</sup>

<sup>1</sup>Institute of Earth Sciences, Faculty of Natural Sciences, University of Silesia in Katowice, Będzińska 60, 41-200 Sosnowiec, Poland; <sup>2</sup>Institute of Geological Sciences, Polish Academy of Sciences, Warsaw, Poland; <sup>3</sup>Faculty of Geology and Geography, Sofia University ‘St. Kliment Ohridski’, 15 Tzar Osvoboditel Blvd., 1504 Sofia, Bulgaria and <sup>4</sup>Department of Geology, School of Natural Sciences, Trinity College Dublin, Dublin, Ireland

**Abstract**

Although Variscan terranes have been documented from the Balkans to the Caucasus, the southeastern portion of the Variscan Belt is not well understood. The Strandja Zone along the border between Bulgaria and Turkey encompasses one such terrane linking the Balkanides and the Pontides. However, the evolution of this terrane, and the Late Carboniferous to Triassic granitoids within it, is poorly resolved. Here we present laser ablation – inductively coupled plasma – mass spectrometry (LA-ICP-MS) U–Pb zircon ages, coupled with petrography and geochemistry from the Izvorovo Pluton within the Sakar Unit (Strandja Zone). This pluton is composed of variably metamorphosed and deformed granites which yield crystallization ages of *c.* 251–256 Ma. These ages are older than the previously assumed age of the Izvorovo Pluton based on a postulated genetic relationship between the Izvorovo Pluton and Late Jurassic to Early Cretaceous metamorphism. A better understanding of units across the Strandja Zone can now be achieved, revealing two age groups of plutons within it. An extensive magmatic episode occurred *c.* 312–295 Ma, and a longer-lived episode between *c.* 275 and 230 Ma. Intrusions associated with both magmatic events were emplaced into pre-Late Carboniferous basement, and were overprinted by Early Alpine metamorphism and deformation. These two stages of magmatism can likely be attributed to changes in tectonic setting in the Strandja Zone. Such a change in tectonic setting is likely related to the collision between Gondwana-derived terranes and Laurussia, followed by either subduction of the Palaeo-Tethys Ocean beneath Laurussia or rifting in the southern margin of Laurussia, with granitoids forming in different tectonic environments.

**1. Introduction**

The Late Carboniferous to Triassic was marked by the assembly of a significant portion of the European crust, and these tectonic events are critical to our understanding of the amalgamation of Pangaea and its evolution. A key event in the assembly of Pangaea was the collision of Gondwana (and Gondwana-derived terranes) with Laurussia during the Acadian–Variscan–Alleghanian Orogeny in the Late Carboniferous (i.e. McCann, 2008; Stephan *et al.* 2019; Franke *et al.* 2020;). The Variscan Orogen is exposed in Western and Central Europe, but also occurs north of the West African Craton in Morocco and Algeria, and in the Appalachian Mountains in northeastern North America, where it is termed the Alleghanian Orogeny (Michard *et al.* 2010; Stephan *et al.* 2019; Franke *et al.* 2020). To the southeast of the Bohemian Massif in central Europe, the Variscan Belt is either overprinted by younger orogens or covered by sedimentary rocks. However, Variscan basement massifs are known from the Alps, the Carpatho-Balkanides, the Hellenides, parts of the Pontides and further to the east into the Caucasus (Sengör *et al.* 1988; Haydoutov, 1989; Stampfli, 2000; Himmerkus *et al.* 2007; Gawęda & Golonka, 2011; Mayringer *et al.* 2011; von Raumer, 2013; Zulauf *et al.* 2014; Antić *et al.* 2016; Okay & Topuz, 2017; Spahić & Gaudenyu, 2018; Franke *et al.* 2020).

The Strandja Zone straddling the border between Bulgaria and Turkey forms the focus of this study. The Strandja Zone occurs between the Carpatho-Balkanides to the north and west and the Pontides to the east, and has been variously assigned to either zone (e.g. Okay *et al.* 2001; Sunal *et al.* 2006; Aysal *et al.* 2018). It contains a series of units related to the Variscan and Alpine orogens, and is key to a better understanding of the Variscan Belt in this sector of Pangaea. The post-Variscan evolution of the Strandja Zone is interpreted by many authors as related to the subduction of the Palaeo-Tethys Ocean beneath the southern margin of Laurussia (e.g. Natal'in *et al.* 2016; Aysal *et al.* 2018; Bonev *et al.* 2019a). The Palaeo-Tethys Ocean remained open to the south of the Variscan Belt until the late Palaeozoic, and then the initiation

© The Author(s), 2021. Published by Cambridge University Press. This is an Open Access article, distributed under the terms of the Creative Commons Attribution licence (<http://creativecommons.org/licenses/by/4.0>), which permits unrestricted re-use, distribution and reproduction, provided the original article is properly cited.

**CAMBRIDGE**  
UNIVERSITY PRESS

of northward subduction led to the final closure of the Palaeo-Tethys Ocean in the Middle Triassic (Sengör, 1979, 1984; Sengör *et al.* 1988; Zulauf *et al.* 2014). Furthermore, this northward subduction likely triggered rifting and the opening of back-arc basins along the Laurussian margin, e.g. the Maliac and Kure basins (e.g. Stampfli, 2000; Stampfli & Kozur, 2006).

The Variscan Belt in Europe is characterized by an abundance of granitoids (e.g. Bonin *et al.* 1998; McCann, 2008). Many of the granitoids in the Variscan Belt of southeastern Europe remain undated and intrude into poorly characterized basement which was also affected by Alpine metamorphic overprinting of variable intensity. In this study, we present the first laser ablation – inductively coupled plasma – mass spectrometry (LA-ICP-MS) U–Pb zircon ages and geochemical results from one of the largest intrusive bodies in the Sakar Unit of the Strandja Zone: the Izvorovo Pluton. The emplacement of this pluton was interpreted by Ivanov *et al.* (2001) and Gerdjikov (2005) as the heat source for Late Jurassic to Early Cretaceous metamorphism in the Sakar Unit of the Strandja Zone. Bonev *et al.* (2019a), however, regarded the pluton as Carboniferous based on ages from the Ustrem Pluton. Therefore, obtaining accurate and precise U–Pb geochronological data for the Izvorovo Pluton is a critical test of this interpretation. The new ages of the Izvorovo Pluton are also coupled with petrographic and geochemical data, and integrated with a compilation of published data from the surrounding plutonic suites of the Strandja Zone. Such a data compilation allows us to demonstrate two major magmatic events in the Late Carboniferous and Permian–Triassic. It also allows for better understanding and correlation of the units within the Strandja Zone and across the region.

## 2. Geological setting

The Strandja (or Strandzha) Zone, also known as the Sakar–Strandja Zone (SSZ; Boyadiev & Lilov 1972; Ivanov, 2017), Strandja (Strandzha) Massif (SM; Okay *et al.* 2001; Natal'in *et al.* 2016 and references therein) or Istranca Massif (Bedi *et al.* 2013), is a NW–SE-trending mountain belt, located in the border area between Bulgaria and Turkey (Fig. 1). To the south, the Strandja Zone is covered by Cenozoic sedimentary rocks of the Thrace Basin. The relationship between the Rhodope Metamorphic Complex to the west and the Strandja Zone is poorly understood, and their contact is mostly covered by Cenozoic sedimentary rocks.

### 2.a. Units

In Bulgaria, the Strandja Zone is defined as a pre-Late Cretaceous orogen, that is covered by sedimentary rocks and intruded by plutons related to the formation of Apuseni–Banat–Timok–Sredna Gora Late Cretaceous magmatic arc (Chatalov, 1990; Gallhofer *et al.* 2015). A key feature of the Strandja Zone is that the main phase of deformation and metamorphism occurred during the Late Jurassic to Early Cretaceous. This event is known as the Early Alpine Orogeny in Bulgarian literature (i.e. Ivanov *et al.* 2001), and the Cimmerian Orogeny in Turkish literature (i.e. Cattò *et al.* 2018). Based on their structural position during the Early Alpine Orogeny, the degree of metamorphism and stratigraphic characteristics, three units have been defined in the Bulgarian part of the Strandja Zone: the Sakar, Strandja and Veleka units (Chatalov, 1990; Gerdjikov, 2005).

The Sakar Unit is exposed within the Sakar Mountains, but also continues westward of the Maritsa River into the Harmanli Block west of Harmanli, as well as the Maritsa region (Fig. 1). The

Strandja Unit is located to the east of the Sakar Unit, within the Strandja Mountains and Derwent Heights along the Bulgarian–Turkish border, and further to the southeast in Turkey towards the vicinity of Istanbul. The Veleka Unit is an allochthon of the Zubernovo Nappe (Chatalov, 1990), that has been emplaced over the less intensely metamorphosed Strandja Unit itself (Gerdjikov, 2005).

### 2.b. Evolution of the units and the granitoids

The Sakar and Strandja units share a similar geological history (e.g. Chatalov, 1990). Late Carboniferous to Triassic granitoids and meta-granitoids in both units were intruded into metamorphic basement, which is composed of gneisses, schists and amphibolites. This pre-Late Carboniferous basement includes Neoproterozoic–Cambrian (Natal'in *et al.* 2016) and Ordovician (Bonev *et al.* 2019a) felsic magmatic rocks, and is considered to represent peri-Gondwanan terrane(s) that formed along the northern Gondwanan margin (e.g. Stampfli, 2000; Okay & Topuz, 2017). Late Carboniferous to Triassic magmatism forms significant parts of the Strandja Zone, with the most important batholiths and plutons shown in Figure 1, along with smaller unnamed intrusions within the basement. One of the largest magmatic bodies in the Sakar Unit is the Late Carboniferous Sakar Batholith (~450 km<sup>2</sup>, Kamenov *et al.* 2010; Peytcheva *et al.* 2016; Bonev *et al.* 2019a; Pristavova *et al.* 2019). Neighbouring intrusions include the Late Carboniferous Ustrem Pluton and Melnitsa Complex (Bonev *et al.* 2019a), and the Izvorovo and Levka plutons which are less extensively studied.

The Izvorovo Pluton was defined as a weakly deformed body of equigranular granites, very similar to the intrusive bodies from the Sakar Pluton (Kouzhokharov & Kouzhokharova, 1973). According to the same authors, these granites, with an assumed Precambrian age, may have been emplaced into the lower part of the metamorphic basement represented by migmatitic paragneisses. Based on detailed field mapping and microfabric data, Ivanov *et al.* (2001) significantly enlarged the areal extent of the Izvorovo Pluton by including strongly foliated K-feldspar porphyritic and equigranular granites, previously regarded as the local country rock. Between 1999 and 2000, the westernmost part of the Sakar Mountains and the Harmanli Block area was mapped at 1:25 000 scale. It was demonstrated by Jordanov *et al.* (2008) that this mapped region is almost entirely composed of metamorphosed and deformed granitoids (orthogneisses) of the Izvorovo Pluton in the Sakar area. Due to the extensive Cenozoic cover, the true extent of the Izvorovo Pluton cannot be easily ascertained, but field mapping indicates that the pluton extends westward toward the area south of Haskovo, thus allowing a crude estimate of the areal extent of the pluton at ~500 km<sup>2</sup>. Based on these field constraints, the Harmanli Block is regarded as the western part of the Izvorovo Pluton.

In the Sakar Unit, the metamorphic basement and the Late Carboniferous to Triassic granitoids and meta-granitoids are overlain by Permian to Triassic meta-sedimentary rock of the Topolovgrad Group (Fig. 1; e.g. Chatalov, 1990). All these units are penetratively deformed and metamorphosed during the Late Jurassic to Early Cretaceous Early Alpine Orogeny (Chatalov, 1988, 1990; Gerdjikov 2005; Bonev *et al.* 2020b; Szopa *et al.* 2020). The highest grades (amphibolite-facies) associated with Early Alpine metamorphism are encountered in the Sakar Mountains (Chatalov, 1990; Tsankova & Pristavova 2007a, b) and in the Harmanli Block (Jordanov *et al.* 2008) of the Sakar Unit. Elsewhere within the Sakar Unit, metamorphism was within the greenschist facies. This spatial distribution of higher peak

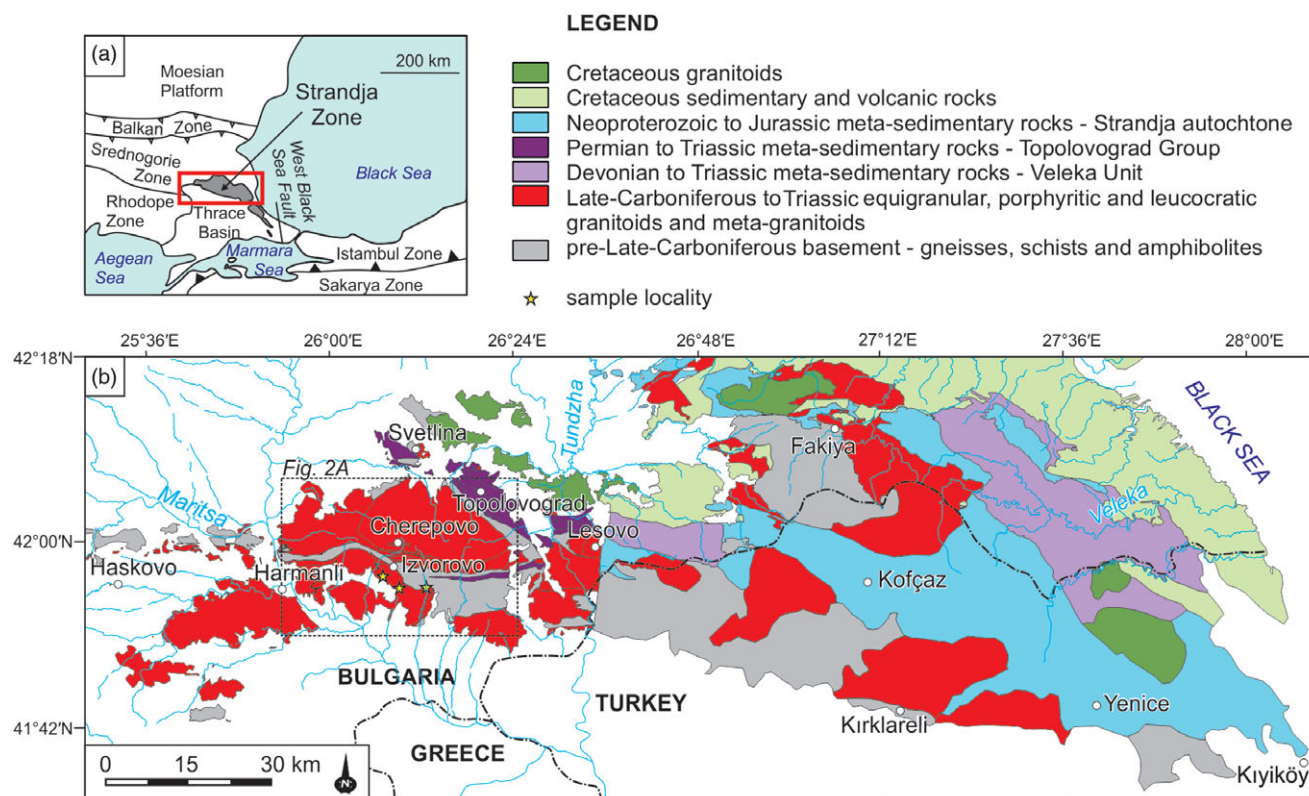


**Fig. 1.** (Colour online) Maps of the Strandja Zone along the Bulgarian–Turkish border: (a) Strandja Zone and surrounding major tectonic units; (b) geological map of the Strandja Zone with the sample localities (modified after Okay *et al.* 2001; Gerdjikov, 2005; Natal'in *et al.* 2016).

metamorphic temperatures compared to the rest of the Sakar Unit of the Strandja Zone led Chatalov (1990) to propose the existence of the so-called Sakar palaeothermal dome. Subsequently, Ivanov *et al.* (2001) and Gerdjikov (2005) argued that these anomalously high temperatures were caused by syn-kinematic Late Jurassic to Early Cretaceous emplacement of large plutonic bodies (i.e. the Sakar, Izvorovo and Varnik plutons). However, new geochronological data have shown that the Sakar Batholith was emplaced in the Late Carboniferous to Early Permian (*c.* 305 – *c.* 295 Ma; Peytcheva *et al.* 2016; Bonev *et al.* 2019a; Pristavova *et al.* 2019). Obtaining accurate and precise U–Pb geochronological data for the Izvorovo Pluton is a further test of this hypothesis.

### 3. Sample localities

The region investigated in the Izvorovo Pluton is located to the south of Izvorovo Village. The Izvorovo Pluton is separated from the Sakar Batholith by an east–west-trending belt of basement rocks (Fig. 2a). The Izvorovo Pluton consists of foliated porphyritic and equigranular meta-granites and porphyroclastic gneisses referred to as the Lesovo Orthometamorphic Complex (Kamenov *et al.* 2010) or described as the ‘Sakar-type’ schistose granites of the Izvorovo Dome (Dimitrov 1956, 1959; Boyanov *et al.* 1965; Ivanov *et al.* 2001). The absolute age of the Izvorovo Pluton has not been determined by isotopic dating, and there is also a lack of any other geochemical and mineralogical data from this pluton. A recent study by Bonev *et al.* (2019a) regarded the Izvorovo Pluton as a part of the Carboniferous Lesovo Complex (gneisses and granites), with an age of *c.* 306 Ma, based on U–Pb zircon dating of meta-quartz–diortite collected from the Ustrem Pluton southeast of Lesovo Village.

In this study, three samples of orthogneiss (SAK-40), augen gneiss (SAK-41) and weakly foliated granite (SAK-42) were collected from the Izvorovo Pluton (Fig. 2). All of these samples represent different types of the Izvorovo meta-granites. The weakly foliated equigranular meta-granite sample SAK-42 is one of the variations of the Izvorovo Pluton, regarded as the ‘Lesovo-type’ pre-metamorphic granite (Kozhoukharov & Kozhoukharova, 1973). The orthogneiss sample SAK-40 and augen gneiss sample SAK-41 are other types of porphyritic meta-granite within the Izvorovo Pluton. However, our field observations showed that significant strain variations occur between the massive, weakly foliated sample SAK-42 and gneiss samples SAK-40 and SAK-41, as the latter are strongly sheared due to their proximity to the country-rock contact.

Sample locations, rock types and mineral assemblages are listed in Table 1. The sample of orthogneiss with feldspar porphyroclasts (SAK-40) was collected from outcrop in a river valley *c.* 1 km to the west of Mladinovo (Fig. 2a, b). The contact between orthogneiss and deformed amphibolite with leucosome layers (basement rock) is observed in the vicinity of this sample locality (*~*200 m to the north). The orthogneiss with feldspar porphyroclasts shows a strong resemblance to porphyritic granitoids from the Sakar Batholith, but is more deformed. The augen gneiss sample (SAK-41) was collected from a large outcrop (*~*3000 m<sup>2</sup>) of pinkish felsic gneisses in the northern part of Oryahovo Village. This rock contains feldspar porphyroclasts up to 3–4 cm in length (Fig. 2a, c). Samples of meta-granite (SAK-42) were collected from an outcrop in close proximity to a dam located *c.* 2 km to the southwest of Izvorovo itself. This meta-granite is equigranular and coarse-grained (Fig. 2a, d). As the Sakar Mountains study area is covered by steppe, the rock outcrops are usually strongly weathered outside of quarries. However, the freshest rock samples were collected for this study.

**Table 1.** Sample localities and modal mineral assemblages

Sample	Lithology	Locality	Latitude	Longitude								
SAK-40	Orthogneiss with feldspar porphyroclasts	W Mladinovo	41° 56' 11.7" N	26° 13' 05.8" E								
SAK-41	Augen gneiss	Oryahovo	41° 55' 34.4" N	26° 09' 35.7" E								
SAK-42	Meta-granite	SW Izvorovo	41° 56' 59.9" N	26° 07' 13.7" E								
Mineral assemblage												
Sample	Qz	Pl	Afs	Bt	Ms	Zrn	Ap	Ttn	Mnz	Fe-ox	Mag	Ilm
SAK-40	***	***	***	**	**	•	•			•	•	
SAK-41	***	***	***	**	**	•	•	•	•			•
SAK-42	***	***	***	**	**	•	•		•	•		

Major (\*\*\*) , minor (\*\*) and accessory (•) amounts of minerals. Qz, quartz; Pl, plagioclase; Afs, alkali feldspar; Bt, biotite; Ms, muscovite; Zrn, zircon; Ap, apatite; Ttn, titanite; Mnz, monazite; Fe-ox, Fe-oxides; Mag, magnetite; Ilm, ilmenite.

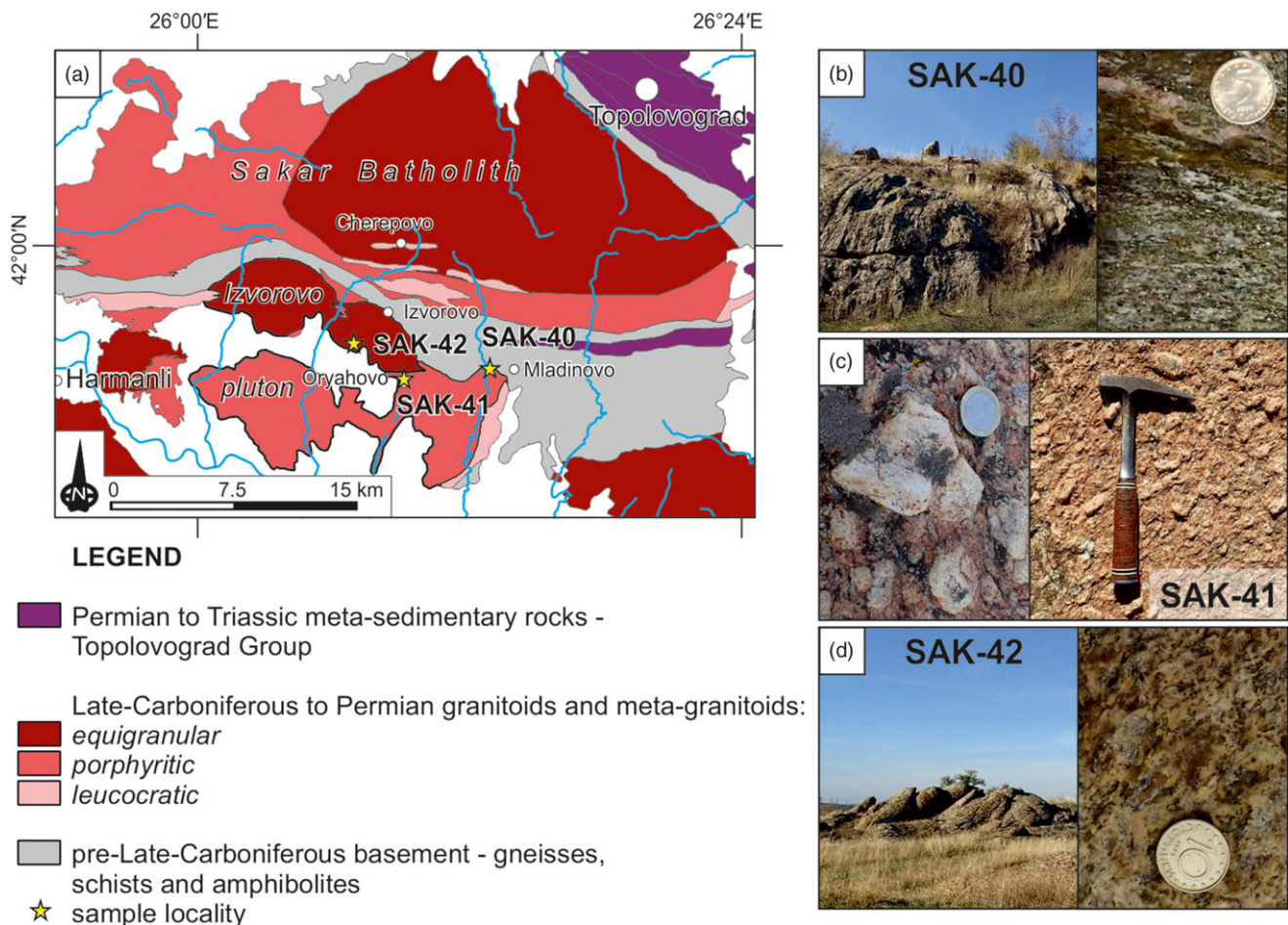


**Fig. 2.** (Colour online) Sample localities in the Izvorovo Pluton: (a) geological map of the Sakar Unit (modified after Okay et al. 2001; Gerdjikov, 2005; Natal'in et al. 2016); (b) strongly deformed orthogneiss with feldspar porphyroblasts (sample SAK-40), from the west of Mladinovo; (c) augen gneiss from which sample SAK-41 was collected from Oryahovo; (d) meta-granite (sample SAK-42) from southwest of Izvorovo.

## 4. Analytical procedures

### 4.a. Sample preparation

Three rock samples (SAK-40, SAK-41, SAK-42) were analysed in this study. Thin-sections were made from each sample and then petrographic observations in transmitted and reflected light were made using an Olympus BX-51 optical polarizing microscope at

the Institute of Earth Sciences, University of Silesia in Katowice, Poland. This was followed by scanning electron microscopy using back-scattered electron (BSE) imagery coupled to an energy-dispersive spectrometry (EDS) using a ThermoFisher Scientific Phenom XL Scanning Electron Microscope (SEM).

For whole-rock geochemistry, all weathered material was removed from the samples, and the most homogeneous parts were

selected. The samples were then crushed using a jaw crusher before being pulverized in an agate ball mill to a powder. A representative aliquot was then despatched for analysis of major and trace elements at the Bureau Veritas Analytical Laboratories in Vancouver, Canada, after being coned and quartered. The litho-geochemical package selected included X-ray fluorescence (XRF) spectrometry for major elements and solution ICP-MS for trace elements, including rare earth elements (REE). Loss on ignition (LOI) on each sample was determined to obtain the volatile content. The resultant geochemical data were then plotted using the GeoChemical Data toolkit (GCDkit) of Janoušek *et al.* (2016).

Separation of zircon was undertaken at the Sample Preparation Laboratory, Institute of Geological Sciences, Polish Academy of Sciences, Kraków, Poland. These separations were made using conventional density separation techniques (i.e. crushing, sieving through a 0.315 mm mesh, washing and panning). Using a standard binocular microscope, zircon was then isolated from other accessory heavy minerals and placed into epoxy resin mounts of 25 mm diameter. The mounts were subsequently ground and the zircon grains polished to half thickness to expose their cores. Prior to U–Pb isotopic analyses, all zircon grains were imaged in transmitted and reflected light microscopy using the same Olympus BX-51 microscope, followed by scanning electron microscopy to reveal their internal textures for spot selection. Scanning electron microscopy was also undertaken with a Thermo Fischer Scientific Phenom XL SEM for BSE imagery of the zircon grains. Additionally, the zircon grains in the epoxy mounts were imaged by cathodoluminescence (CL) on a FET Phillips 30 SEM using a 15 kV accelerating voltage and a beam current of 1 nA to highlight the internal structures of the zircon grains. Prior to CL imaging, the epoxy mounts were carbon-coated. All of the respective petrographic imaging was made at the Institute of Earth Sciences, University of Silesia in Katowice. The carbon coating was then removed and the epoxy mounts were cleaned in an ultrasonic bath before U–Th–Pb isotopic measurements were undertaken.

#### 4.b. Sample analysis

Samples SAK-40, SAK-41 and SAK-42 then underwent U–Th–Pb isotopic analyses at the Department of Geology, Trinity College Dublin, Ireland, using a Photon Machines Analyte Excite 193 nm ArF excimer laser-ablation system with a HelEx 2-volume ablation cell, which was coupled to an Agilent 7900 mass spectrometer. The NIST612 standard glass was used to tune the instruments to obtain a Th/U of unity, and produce low oxide production rates (i.e. ThO<sup>+</sup>/Th<sup>+</sup> typically <0.15 %). A circular laser spot of 24 µm was used, with a repetition rate of 11 Hz. Helium carrier gas was fed into the laser cell at ~0.4 L min<sup>-1</sup>, and was mixed with an aerosol of ~0.6 L min<sup>-1</sup> Ar make-up gas and 11 mL min<sup>-1</sup> N<sub>2</sub>. Eight isotopes (<sup>90</sup>Zr, <sup>202</sup>Hg, <sup>204</sup>Pb, <sup>206</sup>Pb, <sup>207</sup>Pb, <sup>208</sup>Pb, <sup>232</sup>Th and <sup>238</sup>U) were measured during each analysis. These analyses comprised 27.3 s of ablation (300 shots) and 12 s of washout time. The latter portions of the washout time were used for baseline measurements. The ‘VisualAge’ data reduction scheme (Petrus & Kamber, 2012) in the freeware IOLITE package (Paton *et al.* 2011) was used to undertake data reduction of the raw U–Th–Pb isotopic data. Downhole fractionation corrections to the raw data were then made to account for the long-term drift in isotopic or elemental ratios by normalizing all ratios to those of the U–Th–Pb reference materials. Conventional sample-standard bracketing was then applied. The 91500 zircon (<sup>206</sup>Pb–<sup>238</sup>U age of 1065.4 ± 0.6 Ma;

Wiedenbeck *et al.* 1995, 2004) was used as the primary U–Pb calibration standard. The Plešovice zircon (<sup>206</sup>Pb–<sup>238</sup>U age of 337.13 ± 0.37 Ma; Sláma *et al.* 2008) and WRS 1348 zircon (<sup>206</sup>Pb–<sup>238</sup>U age of 526.26 ± 0.70; Poinçon *et al.* 2012) were used as secondary standards, and yielded respective ages of 336.9 ± 2.4 Ma (<sup>206</sup>Pb–<sup>238</sup>U weighted mean age, *n* = 13) and 526.6 ± 3.7 Ma (<sup>206</sup>Pb–<sup>238</sup>U weighted mean age, *n* = 17).

Following isotopic analysis, all analysed zircon grains in the epoxy mounts were again imaged by BSE, and subsequently interpreted using the pre-analysis BSE and CL images to verify any inadvertent mixtures of growth zones in the laser ablation sampling and measurements. The final geochronological calculations, Concordia diagrams as well as weighted mean diagrams were made using the Isoplot 3.75 macro for Microsoft Excel (Ludwig, 2012). In Table S1 (in the Supplementary Material available online at <https://doi.org/10.1017/S0016756821000650>), the data are provided at the 2σ analytical uncertainty level. Weighted mean calculations and discordia intercept ages are also given at the 2σ levels and include decay constant errors. Data with absolute discordance of <5 % (<sup>206</sup>Pb/<sup>238</sup>U vs <sup>205</sup>Pb/<sup>237</sup>U) were treated as concordant data.

## 5. Results

### 5.a. Petrographic observations and whole-rock geochemistry

Sample SAK-40 is the most deformed rock investigated in this study. It was sampled from the area located closest to the orthogneiss – country-rock contact, with the country rock composed of amphibolites and biotite paragneisses. Sample SAK-40 represents a foliated porphyroclastic gneiss (Fig. 2b), which contains quartz, plagioclase, K-feldspar and two micas (muscovite and biotite), with accessory magnetite, as well as various Fe-oxides, zircon and fluoroapatite (Fig. 3a, b). The gneiss has a well-defined foliation, composed of alternating layers of dark minerals (biotite, magnetite and Fe-oxides) and light minerals, mostly quartz and feldspars (Fig. 3a). The deformed porphyroclasts are composed of K-feldspar, are elongated and irregular in shape and are surrounded by fine-grained recrystallized quartz with an undulose extinction.

Sample SAK-41 (Fig. 2c) is an augen gneiss that contains large porphyroclasts of K-feldspar within a quartz, plagioclase and biotite–muscovite matrix, with accessory fluoroapatite, zircon, titanite, monazite and ilmenite (Fig. 3c, d). The K-feldspar has characteristic microcline twinning (Fig. 3d) and is up to 3–4 cm in length. Titanite occurs within nests of co-genetic intergrowths of the two micas (Fig. 3c). The K-feldspar porphyroclasts are interpreted as phenocrysts inherited from the igneous protolith.

Sample SAK-42 is a coarse-grained, equigranular and weakly foliated meta-granite (Fig. 2d), which consists of plagioclase, quartz, K-feldspar, biotite and muscovite with accessory fluoroapatite, zircon, monazite and Fe-oxides (Fig. 3e, f). Accessory minerals occur mostly within randomly distributed, irregular patches of two-mica intergrowths, surrounded by feldspars and quartz. This meta-granite is the least deformed rock sample collected in this study.

Whole-rock major- and trace-element compositions for three samples (SAK-40, SAK-41, SAK-42), and a compilation of the published data from other Late Carboniferous to Early Triassic plutons in the Strandja Zone are presented in Table S2 (in the Supplementary Material available online at <https://doi.org/10.1017/S0016756821000650>). The samples from Izvorovo Pluton are silica-rich (70.4–75.4 wt % SiO<sub>2</sub>) meta-granitoids and orthogneisses, which plot in the granite field on a SiO<sub>2</sub> vs Na<sub>2</sub>O + K<sub>2</sub>O

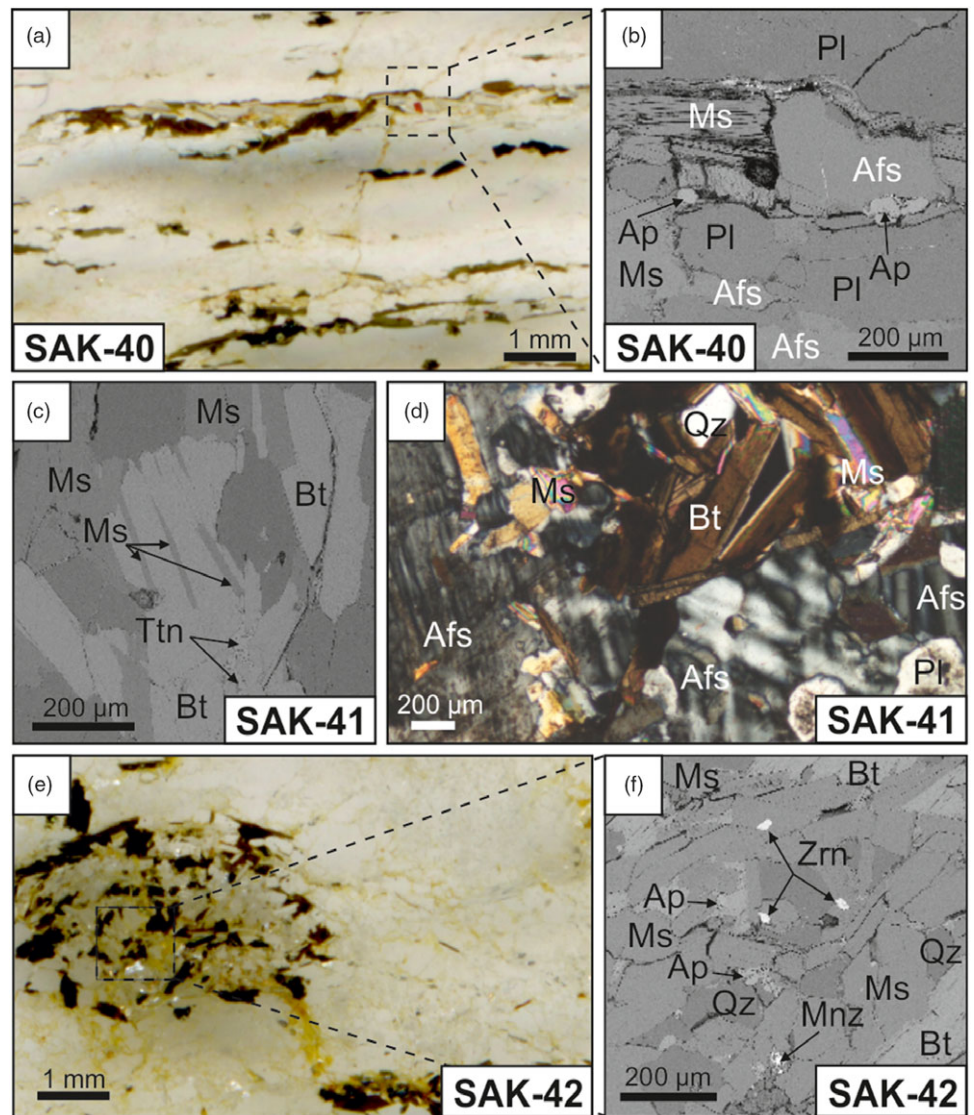


**Fig. 3.** (Colour online) Petrographic images of the gneisses and meta-granite from the Izvorovo Pluton: (a, b) orthogneiss sample SAK-40, (a) thin-section in plane-polarized light (PPL) showing foliation within the orthogneiss, (b) mineral assemblages in the BSE images; (c, d) augen gneiss sample SAK-41, (c) BSE image showing two-mica intergrowths surrounding accessory titanite, (d) thin-section image showing microcline twinning of K-feldspar porphyroclasts (under cross-polarized light); (e, f) meta-granite sample SAK-42, (e) PPL thin-section image showing the coarse-grained textures of the meta-granite, (f) BSE image showing the diverse mineral assemblage of the dark patches surrounded by coarse-grained K-feldspar and quartz. Qz, quartz; Pl, plagioclase; Afs, alkali feldspar; Bt, biotite; Ms, muscovite; Zrn, zircon; Ap, apatite; Ttn, titanite; Mnz, monazite.

diagram (Fig. 4a; Middlemost, 1994), and are peraluminous (Fig. 4b; Shand, 1943). The trace elements were normalized to the ocean-ridge granite (ORG) values of Pearce *et al.* (1984). Samples from the Izvorovo Pluton have similar trace element profiles, characterized by enrichments in K, Rb, Ba, Th and Ce and Sm relative to Ta, Nb, Hf, Zr, Y and Yb (Fig. 4c). These patterns show a resemblance to patterns from the Permian Kirklareli Pluton and Late Carboniferous to Early Permian Sakar Batholith; however, samples from Kirklareli Pluton have stronger negative Ta–Nb anomalies. The rare earth elements (REEs) were normalized to chondrite values of McDonough & Sun (1995; Fig. 4b). The samples show fractionation of the light REE (LREE) relative to heavy REE (HREE), and have negative Eu anomalies (0.31–0.35). These patterns are within the range of samples from Sakar Batholith and Kirklareli Pluton.

### 5.b. U–Pb zircon dating of Izvorovo meta-granitoids

LA-ICP-MS U–Th–Pb isotopic data of the analysed zircons for the samples SAK-40, SAK-41 and SAK-42 are listed in Table S1, in the Supplementary Material available online at <https://doi.org/10.1017/S0016756821000650>. Dates are reported as  $^{206}\text{Pb}$ – $^{238}\text{U}$  ages.

Orthogneiss sample SAK-40 from west of Mladinovo contains oscillatory zoned zircons that are euhedral to subhedral. Zircons are up to 180  $\mu\text{m}$  in length with aspect ratios of 1:1 and 1:2 (Fig. 5a). Some of the zircons have thin rims (up to 8  $\mu\text{m}$  in width), which were not analysed during this study. Thirty-one analyses were made on 30 zircon grains, from which 28 analyses are concordant (<5% disc.; Table S1, in the Supplementary Material available online at <https://doi.org/10.1017/S0016756821000650>; Fig. 6a). From all the concordant data, one analysis is identified as of being a mixture of rim and oscillatory zoned zircon core in BSE and CL post-imaging, and is therefore excluded from further consideration in this study. The remaining data range from c. 248 Ma to c. 440 Ma, with a significant cluster on concordia between c. 248 Ma and c. 262 Ma (Fig. 6a). This cluster of 25 analyses defines a weighted mean  $^{206}\text{Pb}$ – $^{238}\text{U}$  age of  $254 \pm 2$  Ma (MSWD = 1.5; Fig. 6b). This age is interpreted as the crystallization age of the magmatic protolith. Two older analyses come from zircon cores (Fig. 5a) and are interpreted as inherited components.

Augen gneiss sample SAK-41 from Oryahovo contains zircons that are elongated and euhedral to subhedral. Zircons are up to 220  $\mu\text{m}$  in length, with aspect ratios of 1:1 to 4:1 (Fig. 5b). All zircons have strong oscillatory zonation. Some of the grains contain

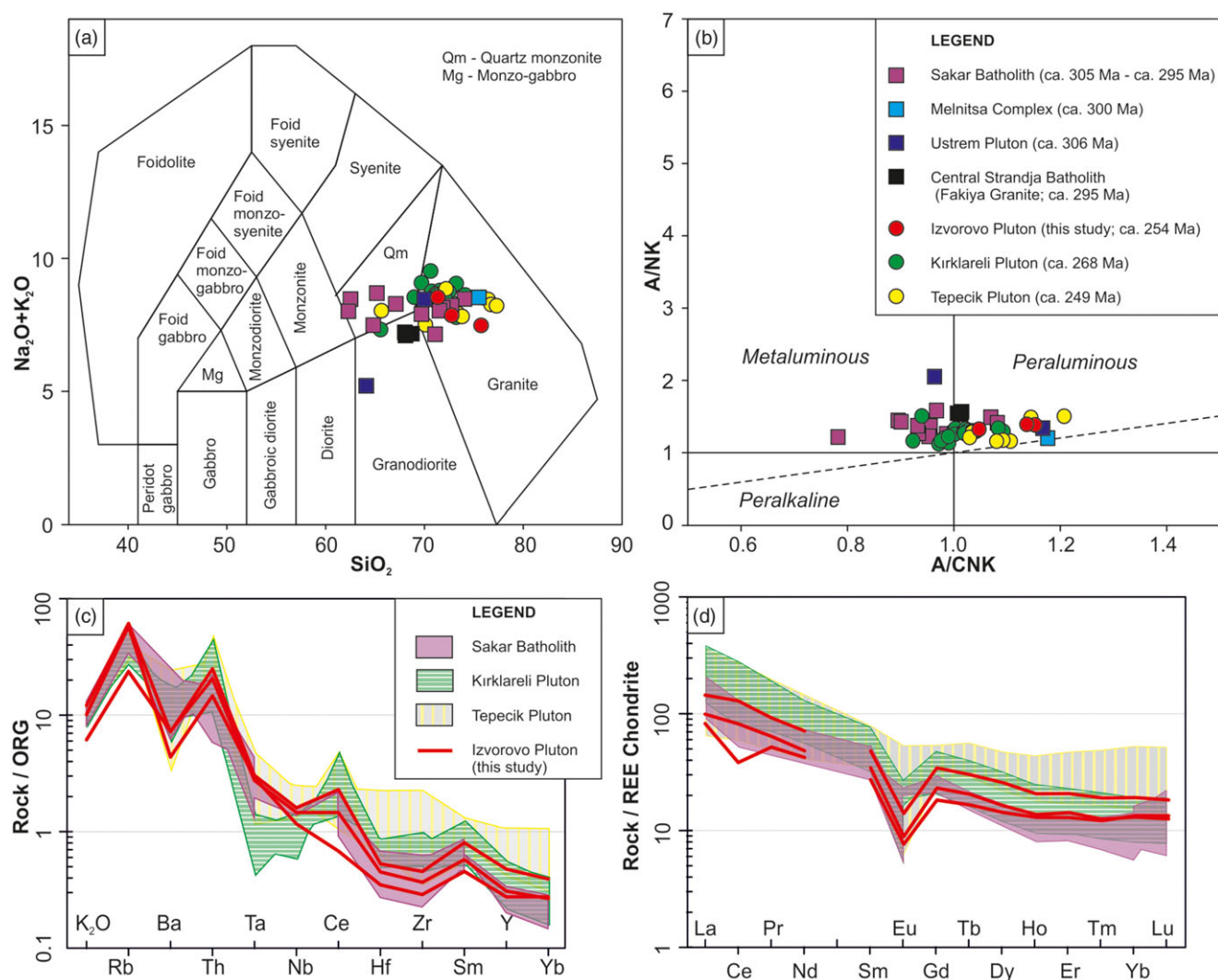


**Fig. 4.** (Colour online) Major and trace elements diagrams for meta-granitoids and gneisses from the Strandja Zone: (a) total alkali vs silica (TAS) diagram (Middlemost, 1994); (b) A/CNK vs A/NK plot of Shand (1943); (c) ocean ridge granite (ORG)-normalized diagram with normalization values after Pearce *et al.* (1984); (d) chondrite-normalized REE diagram with normalization values from McDonough & Sun (1995). Data from previous studies are from: Sunal *et al.* (2006), Kamenov *et al.* (2010), Machev *et al.* (2015), Aysal *et al.* (2018), Bonev *et al.* (2019a), and are given in Table S2 (in the Supplementary Material available online at <https://doi.org/10.1017/S0016756821000650>).

thin rims (~5 to ~10  $\mu\text{m}$  in width), which were not analysed during this study. A total of 32 analyses were obtained from 27 grains (Table S1, in the Supplementary Material available online at <https://doi.org/10.1017/S0016756821000650>; Fig. 6c), of which 30 analyses were concordant (<5% disc.). From all the concordant analyses, nine analyses were excluded from further consideration because they were obtained from mixed domains as revealed by BSE and CL post-analysis imagery. Of the remaining data, 21 data points from 19 grains with concordant  $^{206}\text{Pb}$ – $^{238}\text{U}$  ages ranging from c. 251 Ma to c. 269 Ma define a weighted mean  $^{206}\text{Pb}$ – $^{238}\text{U}$  age of  $256 \pm 3$  Ma (MSWD = 3.5). Although these data scatter beyond analytical uncertainty more than the cluster of data points in sample SAK-40, the calculated ages are within analytical uncertainty between the two samples. Thus, c. 256 Ma is interpreted as the emplacement age of the gneiss protolith.

Meta-granite sample SAK-42 from southwest of Izvorovo contains mostly subhedral, and stubby to elongate zircons (up to 240  $\mu\text{m}$  in length, with aspect ratios of 1:1 to 3:1; Fig. 5c), and exhibiting oscillatory zoning. Some of the zircons have thin rims (up to 8  $\mu\text{m}$  in width), which were not analysed during this study.

Thirty-two analyses from 30 grains were obtained (Table S1, in the Supplementary Material available online at <https://doi.org/10.1017/S0016756821000650>; Fig. 6d), of which two data points were discordant (>5% disc.), and four were identified as mixed zones in post-analytical BSE and CL imaging, and were therefore excluded from further consideration. The remaining 26 data points range from c. 240 Ma to c. 460 Ma, of which 24 analyses scatter along concordia between c. 240 Ma and c. 263 Ma, with a weighted mean  $^{206}\text{Pb}$ – $^{238}\text{U}$  age of  $251 \pm 3$  Ma (MSWD = 3.5). This age is within analytical error of the crystallization age of the orthogneiss igneous protolith (SAK-40), and is interpreted as the crystallization age of the meta-granite. The two older analyses come from zircon cores and are interpreted as inherited components.

## 6. Discussion

### 6.a. Interpretation of geochronology and its regional context

All three samples from the Izvorovo Pluton yielded similar U–Pb zircon ages, ranging between  $251 \pm 3$  Ma and  $256 \pm 3$  Ma, with a

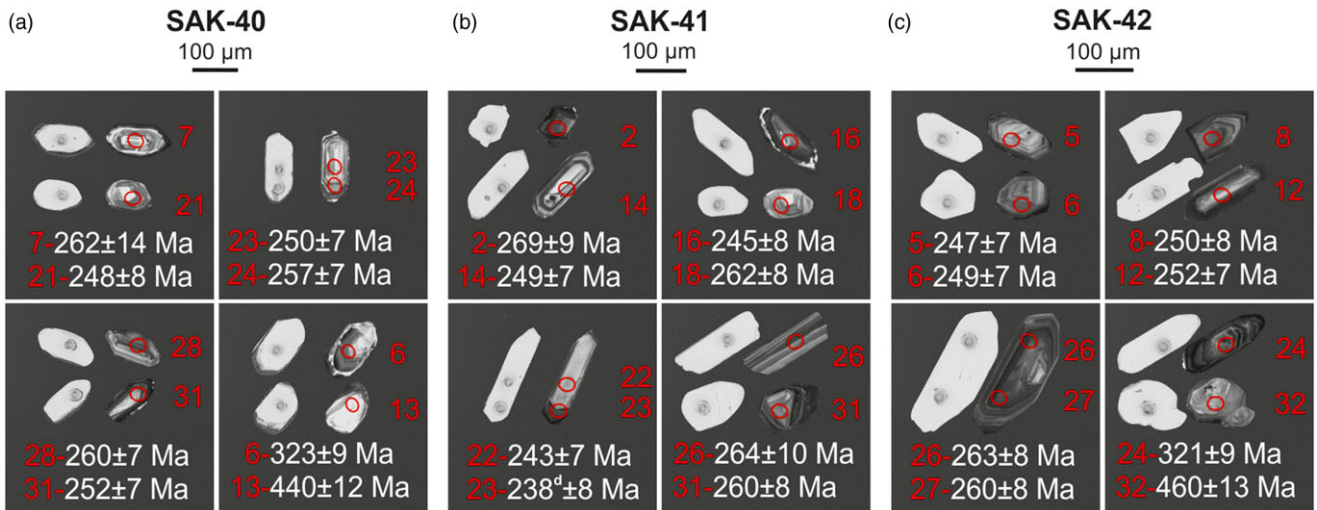


**Fig. 5.** (Colour online) BSE and CL images of representative zircons from: (a) sample SAK-40; (b) sample SAK-41; (c) sample SAK-42. Numbers represent the grain number, reported values are  $^{206}\text{Pb}/^{238}\text{U}$  ages, all presented ages are concordant (<5 % disc.) except for one discordant analysis (denoted d, which is disc. >5 %), and the white circles represent the laser ablation spot.

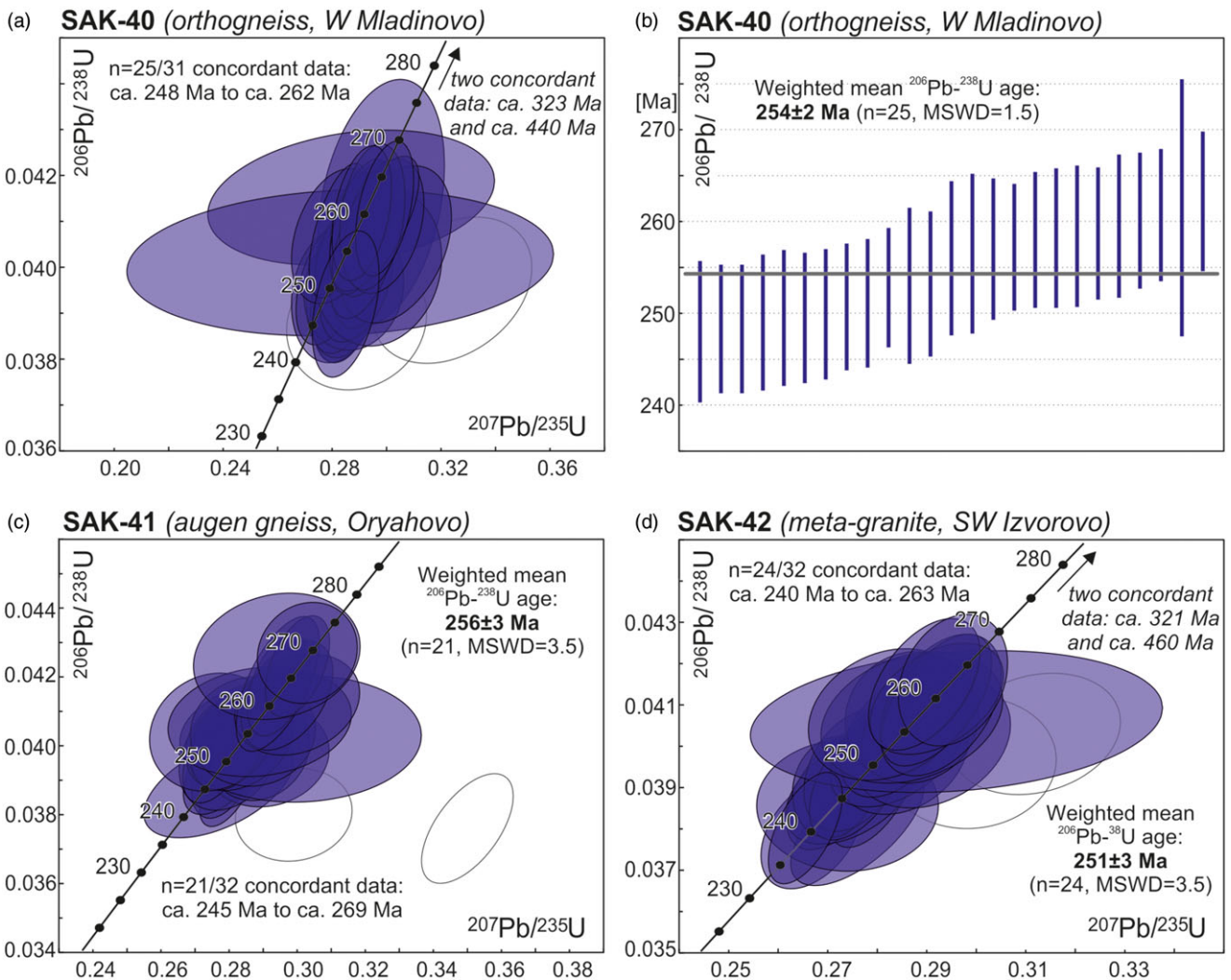


**Fig. 6.** (Colour online) LA-ICP-MS zircon U-Th-Pb analyses for sample: (a, b) SAK-40 (orthogneiss); (c) sample SAK-41 (augen gneiss); (d) sample SAK-42 (meta-granite); Wetherill Concordia diagrams (after Wetherill, 1956) are shown in (a), (b) and (d); the data shown as filled ellipses are used for age calculations, and black ellipses are discordant data (>5 %); analyses of mixed domains are not shown. All data-point error ellipses and error bars are at the  $2\sigma$  uncertainty level.

weighted mean  $^{206}\text{Pb}/^{238}\text{U}$  age of  $254 \pm 5$  Ma. The time interval between  $251 \pm 3$  Ma and  $256 \pm 3$  Ma is considered as the crystallization age of the Izvorovo Pluton. This shows that both varieties of equigranular and porphyritic meta-granite from the Izvorovo Pluton, which used to be regarded as two different units of meta-granite and migmatite (Kozhoukharov & Kozhoukharova, 1973), are coeval. Within the zircon populations of the samples, xenocrysts were detected. Some inherited cores were analysed, and yielded concordant ages at 460–440 Ma and c. 320 Ma (Table S1, in the Supplementary Material available online at <https://doi.org/10.1017/S0016756821000650>). A 460–440 Ma magmatic episode within the Sakar Unit was recently described by Bonev *et al.* (2019a), who dated leucocratic stock meta-granites exposed to the east of the Sakar Batholith at  $462 \pm 3$  Ma. The younger population of zircon xenocrysts is consistent with 320–310 Ma ages obtained from zircons commonly found within the Sakar Batholith (Bonev *et al.* 2019a; Pristavova *et al.* 2019). The 320–310 Ma zircons documented from the Sakar Batholith are interpreted by Bonev *et al.* (2019a) and Pristavova *et al.* (2019) as ‘ante-crysts’, i.e. a group of crystals from an earlier pulse of magma which were incorporated by a later pulse. This suggests the occurrence of at least one earlier magmatic pulse in the Late Carboniferous within the Sakar Unit.

The crystallization age of the Izvorovo Pluton post-dates the emplacement of the Sakar Batholith (305–295 Ma; Peytcheva *et al.* 2016; Bonev *et al.* 2019a; Pristavova *et al.* 2019). Additionally, the Izvorovo Pluton underwent a later Late Jurassic to Early Cretaceous deformation and metamorphic event (Chatalov, 1990; Bonev *et al.*, 2020b), which is clearly visible in outcrop and in the petrographic data obtained from samples SAK-40 and SAK-41. The presented geochronological data invalidate the interpretation of Ivanov *et al.* (2001) and Gerdjikov (2005) that syn-kinematic magmatism (of assumed Late Jurassic to Early Cretaceous age) was the heat source for Early Alpine metamorphism. Thus, the question about the origin of the ‘anomalous’ high-grade metamorphism in the Sakar Mountains relative to the adjacent units remains open.

The Izvorovo Pluton is the first Permian–Triassic plutonic body described within the Sakar Unit, and is clearly emplaced 40 Myr later than Late Carboniferous – Early Permian intrusives such as the Sakar Batholith and coeval intrusions (c. 305 – c. 295 Ma; Peytcheva *et al.* 2016; Bonev *et al.* 2019a; Pristavova *et al.* 2019; Fig. 7; Table S3 in the Supplementary Material available online at <https://doi.org/10.1017/S0016756821000650>). Recently, new U–Pb ages ranging between 245 and 230 Ma were presented for the Harmanli Block Magmatic Complex (Bonev *et al.* 2019b) and St Iliya Heights (near Svetlina; Bonev *et al.* 2020a), located in the southwestern and northern part of the Sakar Unit (Fig. 2a), respectively. This shows that the magmatic evolution of the region is more complex than previously envisaged.

Although the Izvorovo Pluton provides the first evidence of Late Permian magmatism within the Sakar Unit, other Permian and Early Triassic plutons are known from the eastern part of the Strandja Zone. These plutons include the c. 268 Ma Kırklareli Pluton (Aysal *et al.* 2018), the c. 252 Ma Ömeroba Pluton (Natal'in *et al.* 2016; Fig. 7), and the c. 249 Ma Tepecik Pluton, which is located near Istanbul in the southeastern Strandja Zone (Aysal *et al.* 2018). For more detailed information about the published U–Pb zircon ages from Late Carboniferous to Triassic magmatic rocks in the Strandja Zone, see Table S3 in the Supplementary Material available online at <https://doi.org/10.1017/S0016756821000650>. Additionally, there are other published Pb–Pb ages for felsic bodies within the Strandja Unit which

were obtained by the single-zircon stepwise evaporation method (Table S3, in the Supplementary Material available online at <https://doi.org/10.1017/S0016756821000650>; Okay *et al.* 2001; Sunal *et al.* 2006); however, the inability to evaluate various factors (e.g. discordance) in such data means these ages will not be discussed further in this study.

### 6.b. Geochronological and geochemical arguments for two-stage magmatism in the Strandja Zone

Felsic to intermediate intrusive magmatism has played an important role in the crustal evolution of the Strandja Zone, as shown in Figure 7. The new geochronological data from this study and from the literature show that extensive magmatism began in the Late Carboniferous, and is almost continuous until the Triassic in both key components of the Strandja Zone, i.e. the Sakar and Strandja units (Table S3, in the Supplementary Material available online at <https://doi.org/10.1017/S0016756821000650>). The tectonic setting of the Strandja Zone is controversial and depends on the interpreted location of the zone with respect to (1) Variscan collision and (2) the subduction of the Palaeo-Tethys Ocean beneath Laurussia. The first scenario invokes Variscan collision between Gondwana and Laurussia in the granitoid formation (post-collisional granites; post-COLG) in the Strandja Zone. The peri-Gondwana continental magmatic arc, which consisted of the Balkanides, Strandja, Sakarya and Caucasus (BASSAC Block), collided with the Moesia and Istanbul Zone in the Middle Carboniferous (MOIS Block; Okay & Topuz, 2017). Within the Strandja Zone, Variscan metamorphism is observed in the pre-Late Carboniferous basement, which was affected by both Variscan and Early Alpine metamorphism (e.g. Okay *et al.* 2001). The exact age of Variscan metamorphism in the Strandja Zone remains unknown, but it is well established from the Balkanides (c. 340 – 330 Ma; Carrigan *et al.* 2006; Antić *et al.* 2016; Balkanska *et al.* 2021). The second scenario assumes that subduction of the Palaeo-Tethys Ocean beneath Laurussia played a primary role, resulting in various intrusions of volcanic-arc granites (VAG) in the Strandja Zone (Okay *et al.* 2001; Natal'in *et al.* 2016; Peytcheva *et al.* 2016; Aysal *et al.* 2018; Bonev *et al.* 2019a). This scenario is presented by Aysal *et al.* (2018), who suggested subduction-related magmatism with a transition from Permian arc magmatism to Middle Permian – Early Triassic back-arc magmatism. Rift-related felsic magmatism has also been proposed by some authors (i.e. Okay & Nikishin, 2015) for the surrounding regions (e.g. the Western Pontides). Rifting along a continental margin may be associated with back-arc basin development. The sedimentary rocks of the TopoIovgrad Group in the Sakar Unit (Chatalov, 1990; Zagorchev *et al.* 2009) could have been deposited in this basin, which potentially initiated as a back-arc basin located in the northern part of the zone during the Permian–Triassic.

Geochemically, the Late Carboniferous to Early Triassic granitoids of the Strandja Zone are typical of either calc-alkaline volcanic-arc or post-collisional granites. The meta-granitoids from the Strandja Zone (Fig. 8a) plot within the post-collisional granite (post-COLG) field, which overlaps with the volcanic-arc granite (VAG) field on the Rb vs Y + Nb diagram (Pearce, 1996, after Pearce *et al.* 1984). The Rb–Hf–Ta ternary diagram (Harris *et al.* 1986; Fig. 8b) indicates that the Late Carboniferous to Early Permian Sakar Batholith and Late Permian Izvorovo Pluton plot within the collisional granite field, whereas data from the Permian Kırklareli Pluton, and most of the data from the Early Triassic Tepecik Pluton, lie within the VAG field. However, as was

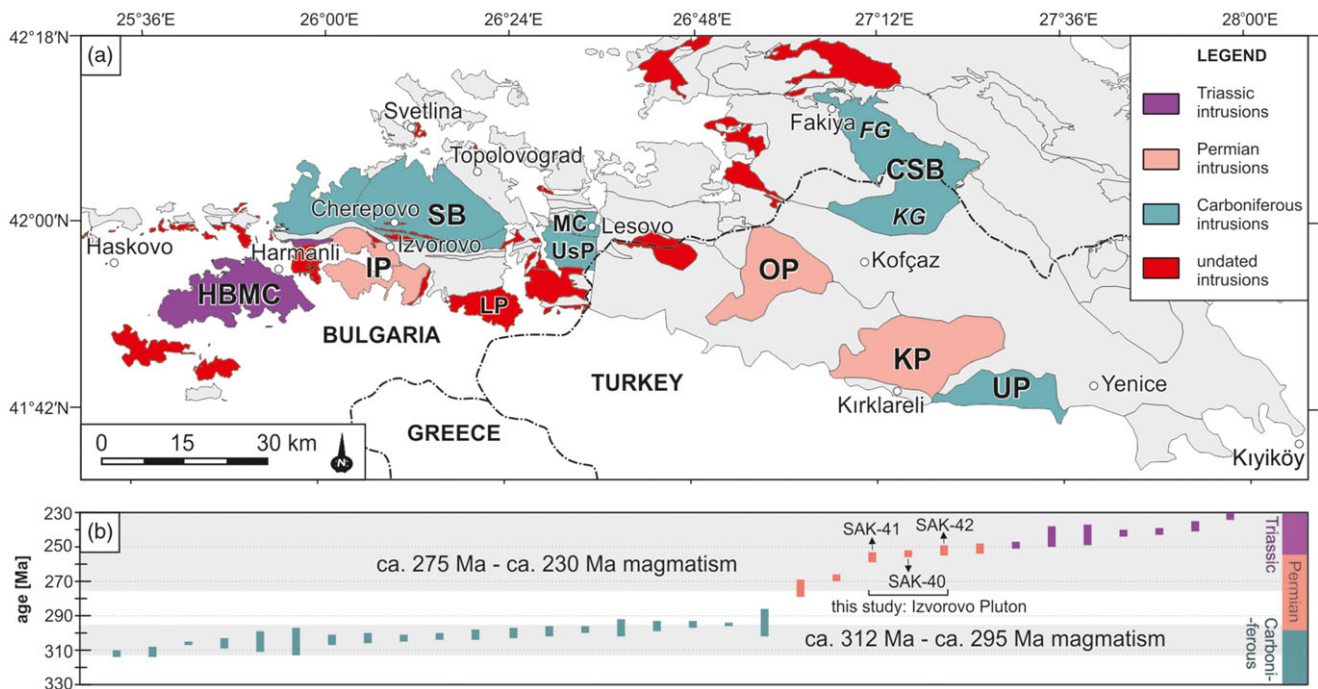


**Fig. 7.** (Colour online) Spatial and temporal distribution of the Late Carboniferous to Triassic magmatic rocks in the Strandja Zone: (a) geological map showing classification of plutonic bodies according to their age of emplacement (HBMC = Harmanli Block Magmatic Complex, IP = Izvorovo Pluton, SB = Sakar Batholith, LP = Levka Pluton, MC = Melnitsa Complex, UsP = Ustrem Pluton, OP = Ömeroba Pluton, KP = Kırklareli Pluton, UP = Üsküp Pluton, CSB = Central Strandja Batholith consisting of FG = Fakiya granite and KG = Kula granite); (b) summary of U–Pb zircon age determinations from all dated plutonic bodies within the Strandja Zone. Data sources are given in Table S3 (in the Supplementary Material available online at <https://doi.org/10.1017/S0016756821000650>).

shown by Harris *et al.* (1986), not all post-COLG magmas demonstrate the degree of Ta enrichment defined by the boundaries in Figure 8b. The geochemical data of the Late Carboniferous to Early Triassic meta-granitoids of the Strandja Zone also do not show a systematic trend in the temporal evolution of the magma chemistry, or in the tectonic setting inferred from those geochemical data. However, this interpretation is only based on empirical assumptions from geochemical diagrams, and can additionally be disturbed by Rb mobilization due to weathering or metamorphism which affected the granitoids.

The Late Carboniferous to Triassic magmatism is assigned by many authors as related to the subduction of the Palaeo-Tethys Ocean beneath the southern margin of Laurussia (Sunal *et al.* 2006; Natal'in *et al.* 2016; Aysal *et al.* 2018; Bonev *et al.* 2019a) with further magmatism in a back-arc setting in the Middle Triassic (Aysal *et al.* 2018). This interpretation is supported by published geochronological data which grouped all the intrusions as a single long-lived magmatic event. However, in this study, two stages (Late Carboniferous and Permian–Triassic) of magmatism in the Strandja Zone are now proposed. The first episode took place in the Late Carboniferous between *c.* 312 Ma and *c.* 295 Ma (Table S3, in the Supplementary Material available online at <https://doi.org/10.1017/S0016756821000650>; Georgiev *et al.* 2012; Machev *et al.* 2015; Natal'in *et al.* 2016; Peytcheva *et al.* 2016; Bonev *et al.* 2019a; Pristavova *et al.* 2019). It started with the intrusion of several small unnamed bodies described from the Kasatura and Kaletpe regions near Kiyiköy in the Strandja Unit (Fig. 1; Natal'in *et al.* 2016), and was followed by extensive emplacement of large plutons between *c.* 305 Ma and 295 Ma, e.g. the Sakar and Central Strandja batholiths. However, the presence of *c.* 320 to *c.* 310 Ma zircon antecrysts within plutonic rocks of the Sakar Batholith, Ustrem Pluton and Melnitsa Complex (Bonev *et al.* 2019a)

suggests that this early-stage magmatism was voluminous within the Strandja Zone. It confirms similarities to neighbouring areas where felsic intrusions with ages of *c.* 320–310 Ma are widespread, e.g. the Sakarya Zone (Ustaömer *et al.* 2012, 2013) and the eastern Mediterranean realm (Meinhold *et al.* 2008). Following the *c.* 312 to *c.* 295 Ma magmatic activity, after *c.* 20 Myr of quiescence, a more extended period of magmatism began in the Permian at *c.* 275 Ma, and which ceased in the Triassic by *c.* 230 Ma. The ages of the granitic bodies from this period are well established from the Strandja Unit (Natal'in *et al.* 2016; Aysal *et al.* 2018), whereas previously there was no evidence of coeval magmatism within the Sakar Unit. However, in this study, *c.* 251 Ma to *c.* 256 Ma ages for the Izvorovo Pluton are documented from the Sakar Unit. Additionally, *c.* 245 Ma to *c.* 230 Ma ages were presented for the Harmanli Block Magmatic Complex and St Iliya Heights (Bonev *et al.* 2019b, 2020a; Fig. 7).

These new data allow for the division of felsic to intermediate magmatism within the Strandja Zone into two age groups: (1) a short Late Carboniferous (*c.* 312 to *c.* 295 Ma) extensive magmatic event; and (2) Permian–Triassic magmatism (*c.* 275 to *c.* 230 Ma; Fig. 7b). These two age groups show significant differences in the characteristics of the zircon populations. The first group of Late Carboniferous granites show that within the population of typical oscillatory-zoned zircons, inherited components and antecrysts play an important role. In the *c.* 298 Ma albitized Sakar granitoid (Kandarata Quarry, Sakar Batholith), a considerable part of the analysed grains yielded ages between *c.* 330 Ma and *c.* 310 Ma, and were interpreted as antecrysts (Pristavova *et al.* 2019). Similar results were obtained from a *c.* 296 Ma porphyritic granite near Planinovo in the Sakar Batholith (sample S14), where half of the concordant zircon data range from *c.* 340 Ma to *c.* 310 Ma, and were interpreted as antecrysts. There is also a minor population

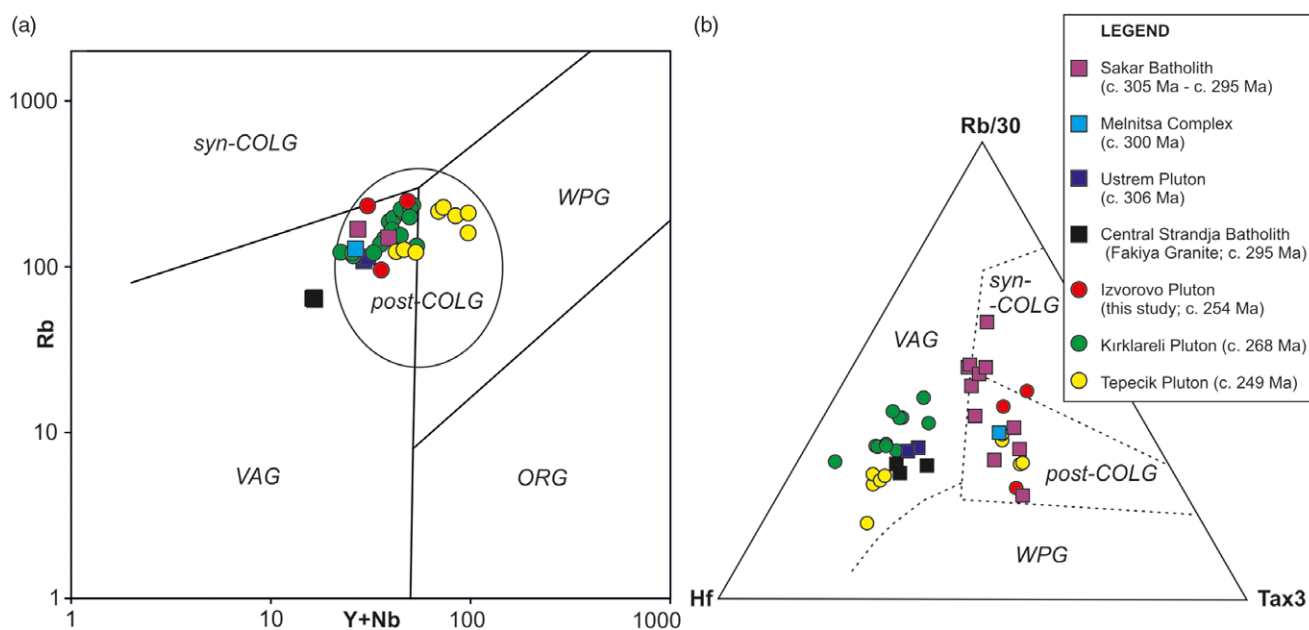


**Fig. 8.** (Colour online) Diagrams for discriminating the tectonic settings of granitic rocks: (a) the Rb-(Y + Nb) diagram (after Pearce, 1996, modified from Pearce *et al.* 1984); (b) the Rb-Hf-Ta ternary diagram (after Harris *et al.* 1986, modified from Pearce *et al.* 1984) distinguishing volcanic-arc granite (VAG), within-plate granite (WPG), syn-collisional granite (syn-COLG) and post-collisional granite (post-COLG). Data from previous studies are from Sunal *et al.* (2006), Kamenov *et al.* (2010), Machev *et al.* (2015), Aysal *et al.* (2018), Bonev *et al.* (2019a) and are given in Table S2 (in the Supplementary Material available online at <https://doi.org/10.1017/S0016756821000650>).

of xenocrysts (at c. 556 Ma and c. 636 Ma; Bonev *et al.* 2019a). A c. 295 Ma equigranular granite (Balgarska Polyana, Sakar Batholith, sample S4), dated by Bonev *et al.* (2019a), also contains abundant xenocrystic material (almost half of the concordant data) within the zircon population, with a broad age spectrum between c. 600 Ma and c. 370 Ma. The dominance of 330–310 Ma antecrysts within zircon populations was also detected from a c. 306 Ma meta-quartz diorite from the Ustrem Pluton (sample S36) and a c. 300 Ma porphyritic meta-granite from the Melnitsa Complex (sample S18), where they represent ~80 % of the concordant data (Bonev *et al.* 2019a). Because Late Carboniferous granitoids contain a large spectrum of components inside the zircon population, with a variety of ages ranging between c. 600 Ma and 305–295 Ma (the age of intrusion), the group can be classified as inheritance-rich granitoids.

On the other hand, the second group of Permian–Triassic intrusions do not contain a significant amount of antecrysts and xenocrysts. Aysal *et al.* (2018) showed that the zircon population of the c. 268 Ma Kirklareli meta-granite (sample KG-1) contained only a few inherited cores. Another study published by Natal'in *et al.* (2016) showed that within the zircon population of a c. 244 Ma leucocratic dyke cutting the Kirklareli Pluton (sample KI-231), all of the xenocrysts have an age directly related to the age of Kirklareli Pluton. This age range is between c. 270 Ma and c. 250 Ma, and therefore probably comes from assimilation of the host rock. A sample of c. 252 Ma porphyritic meta-granite from Ömeroba Pluton (KI-233.3) contains only two xenocrysts, with ages of c. 360 Ma and c. 330 Ma, respectively (Natal'in *et al.* 2016). A c. 249 Ma meta-granitoid from Tepecik Pluton (sample CT-23) had no xenocrysts or antecrysts (Aysal *et al.* 2018). Samples from Izvorovo Pluton contain only a few xenocrysts dated at c. 440 Ma and c. 323 Ma (sample SAK-40) and at c. 460 Ma and c. 321 Ma (SAK-42), respectively. The Permian–Triassic group represents inheritance-poor granitoids.

Zircon saturation temperatures ( $T_{Zr}$ ) calculated from bulk-rock compositions (after Watson & Harrison, 1983; Table S2, in the Supplementary Material available online at <https://doi.org/10.1017/S0016756821000650>) were used to estimate temperatures at which the magma solidified. The temperature calculated for the Sakar Batholith ranges between 717 °C and 805 °C (with average of 760 °C), and for other Late Carboniferous intrusions it is in the range 760–811 °C (with an average of 775 °C). The calculation for Permian Kirklareli Pluton and Triassic Tepecik Pluton yielded temperatures between 778 °C and 852 °C (mean of 805 °C) and 766 °C and 851 °C (mean of 810 °C, excluding one outlier of 932 °C), respectively. The zircon saturation temperatures for Permian Izvorovo Pluton from this study vary between 756 °C and 787 °C (mean of 768 °C). Therefore the Late Carboniferous granitoids with abundant inheritance yield lower  $T_{Zr}$  than inheritance-poor Permian–Triassic rocks with the exception of Izvorovo Pluton. According to Miller *et al.* (2003), the zircon saturation temperature should be interpreted in different ways for inheritance-rich and inheritance-poor granitoids. Inherited zircon components present in the granitoids indicate that the source was zircon-saturated and Zr is present mainly in crystals rather than melt, and  $T_{Zr}$  gives the upper limit on magma temperature. The lack of zircon inherited components implies that the source was undersaturated, and therefore the  $T_{Zr}$  calculated for inheritance-poor granitoids indicates a minimum initial magma temperature (Miller *et al.* 2003). This shows significant differences in magma temperatures between the Late-Carboniferous and Permian–Triassic intrusions in the Strandja Zone, because the maximum magma temperatures calculated for the inheritance-rich Late Carboniferous granitoids does not exceed 760 °C (for Sakar Batholith) and 775 °C (for other coeval granitoids), whereas the minimum magma temperatures for Permian–Triassic intrusions are 768 °C, 805 °C and 810 °C for the Izvorovo, Kirklareli and Tepecik plutons, respectively. Miller *et al.* (2003) proposed that there is a fundamentally different

mechanism of melt production between inheritance-rich and -poor intrusions. Inheritance-poor granitoids are interpreted according to currently accepted modes of felsic magma generation (i.e. dehydration melting in the crust; fractionation of mantle melts, with or without crustal contamination) and without incorporation of the inherited component during transport. However, generation of 'colder', inheritance-rich magma requires a source of water to lower the melt temperature, as the most visible mechanism for large-scale melting at temperatures <800 °C is infiltration of a water-rich fluid phase (Miller *et al.* 2003). Therefore, the inheritance-rich Late Carboniferous granitoids in the Strandja Zone were generated in a tectonic setting that did not reach especially high temperatures but was associated with fluid influx. The inheritance-poor Permian–Triassic intrusions were generated in a hotter, less fluid-rich environment; such settings include extensional or transtensional (Miller *et al.* 2003). This may be attributed to a possible change in the tectonic setting across the Carboniferous–Permian boundary.

The Late Carboniferous intrusions from the Strandja Zone invite correlation with the other Variscan post-collisional granites in the Balkanides. As shown by Carrigan *et al.* (2005), the dominant magmatic episode in the Balkanides took place in the interval between *c.* 315 Ma and *c.* 290 Ma. These authors also highlight that the Variscan Orogen in Bulgaria and the surrounding areas does not include an older phase of *c.* 340 Ma to 325 Ma magmatism, which was confirmed by recent work (e.g. Balkanska *et al.* 2021). This implies a similar evolution of the Balkanides and the western part of the Variscan Orogeny exposed in the Iberian Massif, where *c.* 340 Ma to *c.* 325 Ma felsic intrusions are also absent (Dias *et al.* 1998; Fernández-Suárez *et al.* 2000). A correlation between *c.* 315 Ma to *c.* 290 Ma post-collisional magmatism of the Balkanides and the Late Carboniferous meta-granitoids from Strandja Zone was proposed by Peytcheva *et al.* (2016). This interpretation has been disputed by other studies, which grouped together Late Carboniferous and Permian intrusions in the Strandja Zone into one long-lived period of subduction-related magmatism (e.g. Sunal *et al.* 2006; Natalin *et al.* 2016; Aysal *et al.* 2018; Bonev *et al.* 2019a). However, in this study, it is shown that Late Carboniferous to Triassic felsic to intermediate magmatism in the Strandja Zone represents two separate temporal stages. The younger, Permian–Triassic group is attributed to either subduction-related magmatism according to earlier models proposed for the Strandja Zone (i.e. Bonev *et al.* 2019a) or a rift-related setting, e.g. as inferred for the Western Pontides (Okay & Nikishin, 2015), or both, assuming a transition from a Permian arc setting to a Middle Permian – Early Triassic back-arc setting (Aysal *et al.* 2018). A rift-related environment is probably more likely as it may facilitate the high-temperature conditions required for magma generation (Miller *et al.* 2003). A rift-related setting for Permian to Triassic granitoids in the Strandja Zone is supported by the occurrence of a Permian–Triassic sequence of sedimentary rocks in the Topolovgrad Group located in the northeastern part of Sakar Unit (Chatalov, 1990; Zagorchev *et al.* 2009), which potentially have a back-arc basin affinity.

## 7. Conclusions

This study presents the first evidence of Permian magmatism in the Sakar Unit of the Strandja Zone, detected from the *c.* 251 to 256 Ma Izvorovo Pluton dated in this study. These ages disprove the interpretation of the Izvorovo Pluton as a possible heat source for Late Jurassic to Early Cretaceous metamorphism in the Sakar Unit

proposed by Ivanov *et al.* (2001) and Gerdjikov (2005). The Izvorovo Pluton is one of the largest magmatic bodies within the Sakar Unit, which has a complex magmatic evolution. Permian magmatism has already been well documented in the Strandja Unit, therefore this study allows for better correlation between the various magmatic units within the Strandja Zone. The results presented here highlight the significance of long-lived Permian–Triassic magmatism within the Strandja Zone (Fig. 7). The large granitic bodies intruded into pre-Late Carboniferous basement throughout the whole area from the westernmost vicinity of the Strandja Zone near Harmanli, to the southeastern part located close to Istanbul. These plutons consist of variably deformed and metamorphosed granitoids, which show evidence of post-Triassic metamorphism and deformation. However, all the presented data (i.e. field observations, petrography, geochemistry and geochronology), indicate that even the strongly sheared porphyroclastic gneisses preserve their igneous origin. Permian–Triassic magmatism was preceded by Late Carboniferous to Early Permian (*c.* 312 to *c.* 295 Ma) intrusions known from both parts of the Strandja Zone (e.g. the Sakar and Central Strandja batholiths; Table S3, in the Supplementary Material available online at <https://doi.org/10.1017/S0016756821000650>). Between an intensive short-lived Late Carboniferous event and a series of long-lived Permian to Triassic magmatic events, there was *c.* 20 Myr of magmatic quiescence. These two groups were distinguished based on geochronological data, and supported by inherited zircon populations and zircon saturation temperatures.

The two stages of felsic to intermediate magmatism during the Late Carboniferous to Triassic are attributed to changes in tectonic setting. One possible scenario is emplacement of post-collisional Late Carboniferous granitoids associated with the Variscan Orogeny. This was followed by intrusion of Permian–Triassic granitoids connected either with subduction-related or rift-related settings. The subduction-related scenario is in agreement with the interpretation of the Variscan Belt evolution in the Black Sea region (Okay & Topuz, 2017), whereas the rift-related scenario is consistent with models proposed for the western part of Pontides (i.e. Okay & Nikishin, 2015). This emphasizes the significance of the Strandja Zone as a link in the evolution of the Balkanides and Pontides.

**Acknowledgements.** We wish to thank the Editor, Peter Clift, as well as Wolfgang Dörr and two anonymous reviewers for comments which improved the manuscript. This research was supported by a Preludium Grant awarded to A.S. from the National Science Centre (Narodowe Centrum Nauki), NCN, in Poland (grant agreement no. UMO-2018/29/N/ST10/00368). D.C. is supported in part by a research grant from Science Foundation Ireland (SFI) under Grant Number 13/RC/2092 and 13/RC/2092\_P2 and co-funded under the European Regional Development Fund and by PIPCO RSG and its member companies. The authors would like to thank Nikolay Gospodinov for logistical support during the field trip, and Rafał Juroszek for help with the BSE imaging, as well as Alex Kounov for scientific discussions.

**Declaration of interest.** The authors declare none

**Supplementary material.** To view supplementary material for this article, please visit <https://doi.org/10.1017/S0016756821000650>

## References

- Antić M, Peytcheva I, Von Quadt A, Kounov A, Trivić B, Serafimovski T, Tasev G, Gerdjikov I and Wetzel A (2016) Pre-Alpine evolution of a segment of the North-Gondwanan margin: geochronological and geochemical evidence from the central Serbo-Macedonian Massif. *Gondwana Research* 36, 523–44.

- Aysal N, Şahin SY, Güngör Y, Peytcheva I and Öngen S (2018) Middle Permian–Early Triassic magmatism in the Western Pontides, NW Turkey: geodynamic significance for the evolution of the Paleo-Tethys. *Journal of Asian Earth Sciences* **164**, 83–103.
- Balkanska E, Gerdjikov I, Georfiiev S, Lazarova A, Dörr W and Kounov A (2021) Structural and geochronological constraints on the magmatic and tectonic events in the pre-Alpine basement of the central parts of the Balkan fold-thrust belt (Central Stara Planina Mountains, Bulgaria). *International Journal of Earth Sciences* **110**, 1181–211.
- Bedi Y, Vasilev E, Dabovski C, Ergen A, Okuyucu C, Dogan A, Kagan Tekin U, Ivanova D, Boncheva I, Lakova I, Sachanski V, Kuscu I, Tumcay E, Gülnur Demiray D, Soykan H and Cemal Goncuoglu M (2013) New age data from the tectonostratigraphic units of the Istranca ‘Massif’ in NW Turkey: a correlation with SE Bulgaria. *Geologica Carpathica* **64**, 255–77.
- Bonev N, Filipov P, Raicheva R and Moritz R (2019a) Timing and tectonic significance of Paleozoic magmatism in the Sakar unit of the Sakar-Strandzha Zone, SE Bulgaria. *International Geology Review* **61**, 1957–79.
- Bonev N, Filipov P, Raicheva R and Moritz R (2019b) Triassic magmatism along the Maritsa river valley, Sakar-Strandzha Zone, Bulgaria. *Review of the Bulgarian Geological Society* **80**, 56–7.
- Bonev N, Filipov P, Raicheva R and Moritz R (2020a) Triassic magmatism along the Eurasian margin of the Palaeotethys: U–Pb zircon age constraints from the western part of the Sakar-Strandzha Zone, Bulgaria. *EGU General Assembly Conference Abstracts* 9122.
- Bonev N, Spikings R and Moritz R (2020b)  $^{40}\text{Ar}/^{39}\text{Ar}$  age constraints for an early Alpine metamorphism of the Sakar unit, Sakar–Strandzha zone, Bulgaria. *Geological Magazine* **157**, 2106–12.
- Bonin B, Azzouni-Sekkal A, Bussy F and Ferrag S (1998) Alkali-calcic and alkaline post-orogenic (PO) granite magmatism: petrologic constraints and geodynamic settings. *Lithos* **45**, 45–70.
- Boydjiev S and Lilov P (1972) On the K–Ar dating of the South Bulgarian granitoids from Srednogie and Sakar-Strandja Zones. *Proceedings of the Geological Institute, ser. Geochemistry, Mineralogy, Petrography* **26**, 121–220 (in Bulgarian).
- Boyanov I, Kozhoukharov D and Savov S (1965) Geological structure of the southern slope of Sakar Mountain between the villages Radovets and Kostur. *Review of the Bulgarian Geological Society* **26**, 121–34 (in Bulgarian).
- Carrigan C, Mukasa S, Haydoutov I and Kolcheva K (2006) Neoproterozoic magmatism and Carboniferous high-grade metamorphism in the Sredna Gora Zone, Bulgaria: an extension of the Gondwana-derived Avalonian-Cadomian belt? *Precambrian Research* **147**, 404–16.
- Carrigan CW, Mukasa SB, Haydoutov I and Kolcheva K (2005) Age of Variscan magmatism from the Balkan sector of the orogen, central Bulgaria. *Lithos* **82**, 125–47.
- Cattò S, Cavazza W, Zattin M and Okay A (2018) No significant Alpine tectonic overprint on the Cimmerian Strandja Massif (SE Bulgaria and NW Turkey). *International Geology Review* **60**, 513–29.
- Chatalov G (1988) Recent developments in the geology of the Strandzha zone in Bulgaria. *Bulletin of the Technical University of Istanbul* **41**, 433–66.
- Chatalov GA (1990) *Geology of the Strandja Zone in Bulgaria. Geologica Balcanica, series operum singulorum* 4. Sofia: Bulgarian Academy of Sciences, 263 pp. (in Bulgarian).
- Dias G, Leterrier J, Mendes A, Simões PP and Bertrand JM (1998) U–Pb zircon and monazite geochronology of postcollisional Hercynian granitoids from the Central Iberian Zone (northern Portugal). *Lithos* **45**, 349–69.
- Dimitrov S (1956) Die kinetische Regionalmetamorphose der Jurassischen Ablagerungen und Leucogranite in Süd-Ost Bulgarien. *Abhandlungen des XX Internationalen Geologische Kongress. In Mexico*, 327–33.
- Dimitrov S (1959) Kurze Übersicht der metamorphen Komplexe in Bulgarien. *Freiberger Forschungshefte, Reih. C, H.* **57**, 62–72.
- Fernández-Suárez J, Dunning GR, Jenner GA and Gutiérrez-Alonso G (2000) Variscan collisional magmatism and deformation in NW Iberia: constraints from U–Pb geochronology of granitoids. *Journal of the Geological Society* **157**, 565–76.
- Franke W, Ballèvre M, Cocks LRM, Torsvik TH and Żelaźniewicz A (2020) Variscan Orogeny. In *Encyclopedia of Geology*, 2nd edn. London: Academic Press, 338–49.
- Gallhofer D, Von Quadt A, Peytcheva I, Schmid SM and Heinrich CA (2015) Tectonic, magmatic, and metallogenic evolution of the Late Cretaceous arc in the Carpathian–Balkan orogen. *Tectonics* **34**, 1813–36.
- Gawęda A and Golonka J (2011) Variscan plate dynamics in the circum-Carpathian area. *Geodinamica Acta* **24**, 141–55.
- Georgiev S, Von Quadt A, Heinrich C, Peytcheva I and Marchev P (2012) Time evolution of rifted continental arc: integrated ID-TIMS and LAICPMS study of magmatic zircons from the Eastern Srednogie, Bulgaria. *Lithos* **154**, 53–67.
- Gerdjikov I (2005) Alpine metamorphism and granitoid magmatism in the Strandja Zone: new data from the Sakar Unit, SE Bulgaria. *Turkish Journal of Earth Sciences* **14**, 167–83.
- Harris NBW, Pearce JA and Tindle AG (1986) Geochemical characteristics of collision zone magmatism. In *Collision Tectonics* (eds MP Coward and AC Ries), pp. 67–81. Geological Society of London, Special Publication no. 19.
- Haydoutov I (1989) Precambrian ophiolites, Cambrian island arc, and Variscan suture in the South Carpathian–Balkan region. *Geology* **17**, 905–8.
- Himmerkus F, Anders B, Reischmann T and Kostopoulos D (2007) Gondwana-derived terranes in the northern Hellenides. In *4-D Framework of Continental Crust* (eds RDPCM Hatcher Jr, JH McBride and JR Martínez Catalán), pp. 379–90. Boulder, Colorado: Geological Society of America Memoir 200.
- Ivanov Z, Gerdjikov I and Kounov A (2001) New data and considerations about structure and tectonic evolution of Sakar region, SE Bulgaria. *Annuaire de l'Université de Sofia, Geology and Geography* **91**, 35–80 (in Bulgarian).
- Ivanov Ž (2017) *Tectonics of Bulgaria*. Sofia: Sofia University Press, 331 pp. (in Bulgarian).
- Janoušek V, Moyen JF, Martin H, Erban V and Farrow C (2016) *Geochemical Modelling of Igneous Processes: Principles and Recipes in R Language*. New York: Springer Geochemistry.
- Jordanov M, Sarov S, Georgiev ST, Marinova R, Dobrev G, Grozdev V, Balkanska E and Moskovska L (2008) *Explanatory Notes to the Geological Map of the Republic of Bulgaria 1: 50,000 sheet K-35-76-B (Harmanly)*. Sofia: Geocomplex, 60 pp.
- Kamenov BK, Vergilov V, Dabovski C, Vergilov I and Ivchinova L (2010) The Sakar Batholith: petrology, geochemistry and magmatic evolution. *Geochemistry, Mineralogy and Petrology* **48**, 1–37.
- Kozhoukharov D and Kozhoukharova E (1973) Stratigraphy and petrology of the Precambrian metamorphic rocks from the Sakar Mountain. *Bulletin of the Geological Institute – Series Geochemistry, Mineralogy and Petrography* **22**, 193–210 (in Bulgarian).
- Ludwig KR (2012) *Isoplot 3.75: A Geochronological Toolkit for Microsoft Excel*. Berkeley, California: Geochronology Center Special Publication 5.
- Machev PH, Ganey V and Klain L (2015) New LA-ICP-MS U–Pb zircon dating for Strandja granitoids (SE Bulgaria): evidence for two-stage late Variscan magmatism in the internal Balkanides. *Turkish Journal of Earth Sciences* **24**, 230–48.
- Mayringer F, Treloar PJ, Gerder A, Finger F and Shengelia D (2011) New age data from the Dzirula massif, Georgia: implications for the evolution of the Caucasian Variscides. *American Journal of Science* **311**, 404–41.
- McCann T (2008) *The Geology of Central Europe: Volume 1: Precambrian and Palaeozoic*. Geological Society of London, 748 pp.
- McDonough W and Sun SS (1995) The composition of the Earth. *Chemical Geology* **67**, 1050–6.
- Meinhold G, Reischmann T, Kostopoulos D, Lehnert O, Matukov D and Sergeev S (2008) Provenance of sediments during subduction of Palaeotethys: detrital zircon ages and olistolith analysis in Palaeozoic sediments from Chios Island, Greece. *Palaeogeography, Palaeoclimatology, Palaeoecology* **263**, 71–91.
- Michard A, Soulaïmani A, Hoepffner C, Ouanaimi H, Baïdler I, Rjimatî EC and Saddiqi O (2010) The South-Western branch of the Variscan Belt: evidence from Morocco. *Tectonophysics* **492**, 1–24.
- Middlemost E (1994) Naming materials in the magma/igneous rock system. *Earth Science Review* **37**, 215–24.
- Miller CF, McDowell SM and Mapes RW (2003) Hot and cold granites? Implications of zircon saturation temperatures and preservation of inheritance. *Geology* **31**, 529–32.

- Natal'in B, Sunal G, Gün E, Wang B and Zhiqing Y** (2016) Precambrian to Early Cretaceous rocks of the Strandja Massif (northwestern Turkey): evolution of a long lasting magmatic arc. *Canadian Journal of Earth Sciences* **53**, 1312–35.
- Okay A, Nikishin AM** (2015) Tectonic evolution of the southern margin of Laurasia in the Black Sea region. *International Geology Review* **57**(5–8), 1051–1076
- Okay A, Satur M, Tüysüz O, Akyüz S and Chen F** (2001) The tectonics of Strandja Massif: late-Variscan and mid-Mesozoic deformation and metamorphism in the northern Aegean. *International Journal of Earth Science* **90**, 217–33.
- Okay A and Topuz G** (2017) Variscan orogeny in the Black Sea region. *International Journal of Earth Sciences* **106**, 569–92.
- Paton C, Hellstrom J, Paul B, Woodhead J and Hergt J** (2011) Iolite: freeware for the visualisation and processing of mass spectrometric data. *Journal of Analytical Atomic Spectrometry* **26**, 2508–18.
- Pearce J** (1996) Sources and settings of granitic rocks. *Episodes* **19**, 120–5.
- Pearce J, Harris N and Tindle AG** (1984) Trace element discrimination diagrams for the tectonic interpretation of granitic rocks. *Journal of Petrology* **25**, 956–83.
- Petrus JA and Kamber BS** (2012) VizualAge: a novel approach to laser ablation ICP-MS U-Pb geochronology data reduction. *Geostandards and Geoanalytical Research* **36**, 247–70.
- Peytcheva I, Georgiev S and Von Quadt A** (2016) U/Pb ID-TIMS dating of zircons from the Sakar-Strandzha Zone: new data and old questions about the Variscan orogeny in SE Europe. In *Proceedings of the Annual Conference of the Bulgaria Geological Society 'Geosciences 2016'*, pp. 71–72. Sofia: Bulgarian Geological Society.
- Pointon MA, Cliff RA and Chew DM** (2012) The provenance of Western Irish Namurian Basin sedimentary strata inferred using detrital zircon U-Pb LA-ICP-MS geochronology. *Geological Journal* **47**, 77–98.
- Pristavova S, Tzankova N, Gospodinov N and Filipov P** (2019) Petrological study of metasomatic altered granitoids from Kanarata Deposit, Sakar Mountain, southeastern Bulgaria. *Journal of Mining and Geological Sciences* **62**, 53–61.
- Sengör AMC** (1979) Mid-Mesozoic closure of Permo Triassic Tethys and its implications. *Nature* **279**, 590–3.
- Sengör AMC** (1984) The cimmeride orogenic system and the tectonics of Eurasia. *Geological Society of America, Special Paper* **195**.
- Sengör AMC, Altiner D, Cin A, Ustaömer T and Hsü KJ** (1988) Origin and assembly of the Tethyside orogenic collage at the expense of Gondwana Land. Gondwana and Tethys. In *Gondwana and Tethys* (ed. MG Audley-Charles), pp. 119–81. *Geological Society of London, Special Publication* no. 37.
- Shand SJ** (1943) *Eruptive Rocks: their Genesis, Composition, Classification, and Their Relation to Ore-Deposits, with a Chapter on Meteorite*. New York: Wiley.
- Sláma J, Košler J, Condon DJ, Crowley JL, Gerdes A, Hanchar JM, Horstwood MSA, Morris GA, Nasdala L and Norberg N** (2008) Plešovice zircon: a new natural reference material for U–Pb and Hf isotopic microanalysis. *Chemical Geology* **249**, 1–35.
- Spahić D and Gaudenyu T** (2018) Primordial geodynamics of Southern Carpathian-Balkan basements (Serbo-Macedonian Mass): Avalonian vs. Cadomian arc segments. *Proceedings of the Geologists' Association* **130**, 142–56.
- Stampfli GM** (2000) Tethyan oceans. In *Tectonics and Magmatism in Turkey and the Surrounding Area* (eds E Bozkurt, JA Winchester and JDA Piper), pp. 1–23. Geological Society of London, Special Publication no. 173.
- Stampfli GM and Kozur HW** (2006) Europe from the Variscan to the Alpine cycles. In *European Lithosphere Dynamics* (eds DG Gee and RA Stephenson), pp. 57–82. Geological Society of London Memoir **32**.
- Stephan T, Kroner U, Romer RL and Rösel D** (2019) From a bipartite Gondwanan shelf to an arcuate Variscan belt: the early Paleozoic evolution of northern Peri-Gondwana. *Earth-Science Reviews* **192**, 491–512.
- Sunal G, Natal'in BA, Satir M and Toraman E** (2006) Paleozoic magmatic events in the Strandja Massif, NW Turkey. *Geodinamica Acta* **19**, 283–300.
- Szopa K, Sałacińska A, Gumsley AP, Chew D, Petrov P, Gawęda A, Zagórska A, Deput E, Gospodinov N and Banasik K** (2020) Two-stage Late Jurassic to Early Cretaceous hydrothermal activity in the Sakar Unit of southeastern Bulgaria. *Minerals* **10**, 266. doi: 10.3390/min10030266.
- Tzankova N and Pristavova S** (2007a) New data about petrography and mineralogy of garnet-bearing mica schists in the frame of the Sakar pluton, SE Bulgaria. *Comptes rendus de l'Académie bulgare des Sciences* **60**, 159–64.
- Tzankova N and Pristavova S** (2007b) Metamorphic evolution of garnet-bearing schists from Sakar Mountain, southeastern Bulgaria. *Comptes rendus de l'Académie bulgare des Sciences* **60**, 271–8.
- Ustaömer PA, Ustaömer T and Robertson AHF** (2012) Ion probe U–Pb dating of the Central Sakarya Basement: a peri-Gondwana terrane intruded by Late Lower Carboniferous subduction/collision-related granitic rocks. *Turkish Journal of Earth Sciences* **21**, 905–32.
- Ustaömer T, Robertson AHF, Robertson AHF, Ustaömer PA, Gerdes A and Peytcheva I** (2013) Constraints on Variscan and Cimmerian magmatism and metamorphism in the Pontides (Yusufeli–Artvin area), NE Turkey from U–Pb dating and granite geochemistry. In *Geological Development of Anatolia and the Easternmost Mediterranean Region* (eds AHF Robertson, O Parlak and UC Ünlügenç), pp. 49–74. Geological Society of London, Special Publication no. 372.
- Von Raumer JF** (2013) Pre-Mesozoic Alpine basements: their place in the European Paleozoic framework. *GSA Bulletin* **125**, 89–108.
- Watson EB and Harrison TM** (1983) Zircon saturation revisited: temperature and composition effects in a variety of crustal magma types. *Earth and Planetary Science Letters* **64**, 295–304.
- Wetherill GW** (1956) Discordant uranium-lead ages, I. *Eos, Transactions of the American Geophysical Union* **37**, 320–6.
- Wiedenbeck M, Alle P, Corfu F, Griffin WL, Meier M, Oberli FV, Von Quadt A, Roddick JC and Spiegel W** (1995) Three natural zircon standards for U–Th–Pb, Lu–Hf, trace element and REE analyses. *Geostandards Newsletter* **19**, 1–23.
- Wiedenbeck M, Hanchar JM, Peck W, Sylvester P, Valley J, Whitehouse M, Kronz A, Morishita Y, Nasdala L, Fiebig J, Franchi I, Girard J-P, Greenwood RC, Hinton R, Kita N, Mason PRD, Norman M, Ogasawara M, Piccoli PM, Rhede D, Satoh H, Schulz-Dobrick B, Skår O, Spicuzza MJ, Terada K, Tindle A, Togashi S, Vennemann T, Xie Q and Zheng Y-F** (2004) Further characterisation of the 91500 zircon crystal. *Geostandards and Geoanalytical Research* **28**, 9–39.
- Zagorchev I, Dabovski CH and Nikolov T** (2009) *Geology of Bulgaria, Volume II, Part 5: Mesozoic Geology*. Sofia: 'Prof. Marin Drinov' Academic Publishing House, 355 pp. (in Bulgarian).
- Zulau G, Dörr W, Fisher-Spurlock SC, Gerder A, Chatzaras V and Xypolias P** (2014) Closure of the Paleotethys in the External Hellenides: constraints from U–Pb ages of magmatic and detrital zircons (Crete). *Gondwana Research* **28**, 642–67.